Research Article | Vol. 31, No. 8 / 10 Apr 2023 / Optics Express 13447
Optics EXPRESS

Cryogenically cooled Fe:ZnSe-based chirped pulse amplifier at 4.07 µm

Z. Alphonse Marra,[1,2] Yi Wu,[1] Fangjie Zhou,[1] and Zenghu Chang[1,3]

[1]Institute for the Frontier of Attosecond Science and Technology, The College of Optics and Photonics (CREOL) and Department of Physics, University of Central Florida, Orlando, FL 32816, USA
[2]alphonse.marra@ucf.edu
[3]zenghu.chang@ucf.edu

Abstract: A femtosecond chirped pulse amplifier based on cryogenically cooled Fe:ZnSe was demonstrated at 333 Hz—33 times higher than previous results achieved at near-room-temperature. The long upper-state lifetime allows free-running, diode-pumped Er:YAG lasers to be used as pump lasers. 250-fs, 4.59-mJ pulses are produced with a center wavelength of 4.07 µm, which avoids strong atmospheric CO_2 absorption that cuts on around 4.2 µm. It is therefore possible to operate the laser in ambient air with good beam quality. By focusing the 18-GW beam in air, harmonics up to the ninth order were observed indicating its potential for use in strong-field experimentation.

1. Introduction

Since the advent of chirped pulse amplification (CPA) in the 1980s and the advancement of the Ti:Sapphire laser in the 1990s, the near-infrared (NIR, 0.75–1.4 µm) CPA laser centered at 800 nm has been the workhorse for attosecond scientific research based on high harmonic generation (HHG). The cut-off energy of a phase-matched high harmonic spectrum obtained from a Ti:Sapphire source, however, is limited to about 150 eV [1]. The next major step forward for attosecond sources will extend the HHG cut-off energy by taking advantage of wavelength scaling laws via new gain media and nonlinear techniques. With recent advances in ultrafast driving sources in the short-wave infrared (SWIR, 1.4–3 µm) region, attosecond pulses extending into the water window (282–533 eV), in which water is less absorptive than carbon, and beyond have now been demonstrated [2–6], but photon flux has never been high enough for time-resolved study of the oxygen K-edge (533 eV). Efficiently probing electron dynamics beyond the water window and into the keV region will require sources that currently do not exist. Pushing past the SWIR region—into the mid-wave infrared (MWIR, 3–8 µm) region—is made more difficult by the lack of technologically mature optical materials, opto-electronics, and detection methods and by atmospheric absorption at certain wavelengths [7].

Among the most promising ultrafast MWIR sources are optical parametric chirped-pulse amplifiers (OPCPA) pumped at 1 µm and 2 µm and chirped pulse amplifiers (CPA) seeded by optical parametric amplifiers (OPA). OPCPAs based on nonlinear crystals that can be pumped by Yb/Nd-laser-based, 1-µm sources, such as potassium titanyl arsenate (KTA) and lithium niobate (LNB) are responsible for some of the sources with the highest peak powers in the MWIR region, up to an impressive 300 GW. However, repetition rates tend to be low, in the 10–20 Hz range [8–11], although high repetition rate OPCPAs are emerging [7]. Chirped pulse amplification in near-room-temperature (7°C) Fe:ZnSe has successfully yielded 150-fs, 3.5-mJ pulses centered at 4.4 µm, but repetition rate was low at 10 Hz [12]. The seven-pass CPA laser was placed in a vacuum chamber to avoid energy loss and spectral distortion caused by strong CO_2 absorption in the 4.2–4.4-µm region. Due to the short upper-state lifetime of Fe:ZnSe at 7°C (~1 µs), a home-built 40-ns, 10-Hz, Q-switched Cr:Yb:Ho:YSGG laser was used as the

#486837 https://doi.org/10.1364/OE.486837
Journal © 2023 Received 3 Feb 2023; revised 9 Mar 2023; accepted 17 Mar 2023; published 7 Apr 2023

Optics EXPRESS

pump. The average power of the CPA output is 35 mW, which is too low for driving HHG for time-resolved attosecond experiments.

Cryogenically cooling Fe:ZnSe offers several advantages over running at room temperature. First, the upper-state lifetime of Fe:ZnSe peaks at around 80 K, increasing from hundreds of nanoseconds to ~55 µs [13]; therefore, commercially available, free-running microsecond lasers, instead of home-made Q-switched nanosecond lasers, may be used as pumps. Second, the thermal conductivity of Fe:ZnSe is roughly five times higher at 80 K than at room temperature allowing greater heat dissipation during pumping [14]. This reduces thermal lensing, supporting good beam quality. Third, the emission cross section peak of Fe:ZnSe shifts down in wavelength from ~4.3 µm to ~4.1 µm allowing the avoidance of the strong CO_2 absorption lines in atmosphere at roughly 4.2–4.4 µm [15,16]. The aforementioned near-room-temperature Fe:ZnSe experiment implemented a 0.5-Torr vacuum chamber around the entire CPA to avoid beam distortion and absorption [12]. In a later iteration of this source, pulses were produced without a vacuum chamber at 4.5 µm to avoid CO_2 absorption; however, pulse energy was reduced to ~3 mJ and more passes were required [17]. In this article, we detail a 4.07-µm, cryogenically cooled Fe:ZnSe CPA outputting 250-fs, 4.59-mJ pulses at 333 Hz.

2. System details

2.1. Seed generation

The optical layout of the Fe:ZnSe CPA is shown in Fig. 1. It begins with the MWIR seed generation system based on a two-stage OPA. The OPA is pumped by a commercially available, turn-key, Yb-based laser instead of the home-built Cr:Forsterite laser at 1.24 µm as in [12]. The pump pulses originate from a Yb:KGW, 1.025-µm, 100-µJ, 247-fs laser capable of running up to 12-kHz (Light Conversion, Carbide). One third of the pulse energy is converted to the second harmonic (513 nm) via a 1.5-mm beta barium borate (BBO) crystal. A 10-mm bulk yttrium aluminum garnet (YAG) crystal is used to generate a NIR (~1.37 µm) seed via supercontinuum generation. In the first stage of amplification, the NIR light is amplified to 1.38 µJ by 31 µJ of the second harmonic pulse via type-I, non-collinear OPA in a 2-mm BBO crystal. A non-collinear angle (angle between the idler and pump) of 4.2° was chosen to minimize parasitic second harmonic generation (SHG) of the idler [18,19]. In the second stage, collinear difference frequency generation in two 1-mm, fanout, periodically poled lithium niobate (PPLN) chips (HC Photonics Corp.) placed back-to-back between the NIR pulse and 62 µJ of the fundamental (1.025 µm) produces the seed for the CPA with 2.7-µJ, 150-fs pulses at 4.07 µm and up to 12 kHz. Duration was measured using a SHG autocorrelator (APE). After amplification, a 600-line/mm holographic grating (Spectrogon) was used to attenuate the pump by diffracting part of it while effectively acting as a mirror to the MWIR idler pulse. The reflectivity of the grating in this configuration for the MWIR pulse is ~99%. This method of long-pass filtering prevented damage to later optics caused by the intense pump beam and was found to be more practical than using absorptive materials such as germanium or silicon due to nonlinear effects present in those materials under high intensities.

2.2. Chirped pulse amplification in Fe:ZnSe

Pulses are stretched to over 400 ps in an Öffner-style stretcher that is nearly aberration free. The stretcher uses a concave mirror and a convex mirror with radii of curvature 1000-mm and 505-mm respectively and a grating of groove density 240 lines/mm (Richardson Gratings). A 35.5° incident angle was chosen to maximize stretcher throughput efficiency, which was measured to be 75%. Due to gain-narrowing, by the final pass in the multi-pass amplifier, the pulse duration is ~180 ps.

Optics EXPRESS

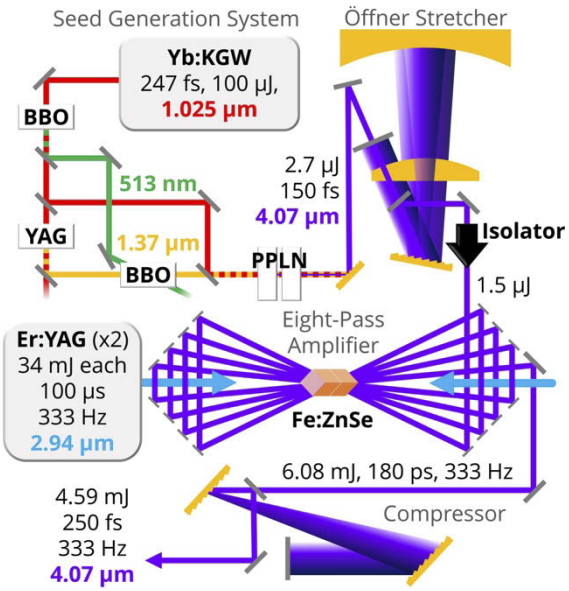

Fig. 1. Diagram of the 4.07-µm CPA with energy, repetition rate, and pulse duration denoted.

Two single-crystal Fe:ZnSe crystals (3photon Ltd.) cut at Brewster's angle (67.5°), with dimensions $8 \times 8 \times 10$ mm^3, and of ion concentration 5×10^{18} cm^{-3} are cooled to 40 K using a close-loop cold-helium circulation system (Cryomech). Vibrations from the helium compressor and cold head are largely eliminated via a 23-ft long, flexible tube transporting compressed helium to a cold finger on which the crystals are mounted. The crystals are situated in a chamber evacuated to 10^{-7} mbar with two CaF_2 windows at Brewster's angle as optical inputs. They are pumped from both sides at 2.94 µm using two 34-mJ, 333-Hz, 100-µs, diode-pumped Er:YAG lasers (Pantec, DPM-50). The repetition rate is more than an order of magnitude higher than the Q-switched, nanosecond laser used in [12]. The 2.94-µm pulses of both lasers are split using a germanium window at Brewster's angle, which acts as a partially polarizing beamsplitter. The polarization vectors of the transmitted beams are rotated 90° by a half-waveplate to make them vertical. This provides a pair of vertically polarized beams on both sides of the chamber to pump the Fe:ZnSe crystals. The four pump beams are roughly flat-top and have a beam diameter of 3.2 mm. The seed beam diameter is 3.1 mm at the $1/e^2$ level at the last pass. Note that the beams are incident on the crystals at Brewster's angle meaning that their actual profiles during amplification are elliptical. With these pump settings, the crystal mount temperature increases slowly until reaching 62 K. Nearly 100% of the pump pulses are absorbed by the crystals. According to simulations, the temperature of the active region of the crystals during operation is 64 K. The rest of the optical components of the CPA system are placed in ambient air, which makes alignment much easier than placing them in a vacuum as in [12].

The seed laser pulses are amplified in an eight-pass bowtie amplifier. Amplified spontaneous emission (ASE) arising from small amounts of fluorescence reflected by various optics in the system became significant as the number of passes through the amplifier was increased. The primary source of the reflection and scattering was determined to be inside the stretcher. A faraday isolator (Thorlabs) was therefore inserted between the stretcher and amplifier to curtail energy-depleting ASE. This addition reduced ASE to ~0.25% of the total output average power, allowing more of the pump energy to be imparted to seed. Figure 2 shows the traces of the ASE and of the amplified pulse itself captured using a HgCdTe detector (Thorlabs) on different scales.

Optics EXPRESS

The red trace shows the amplified pulse as a sharp spike at ~70 μs while ASE is not visible above the background of this trace. This indicates pulse contrast is well over 100. Moreover, the crystal walls were coated with absorptive graphite ink, as has been shown to reduce internal reflections [20].

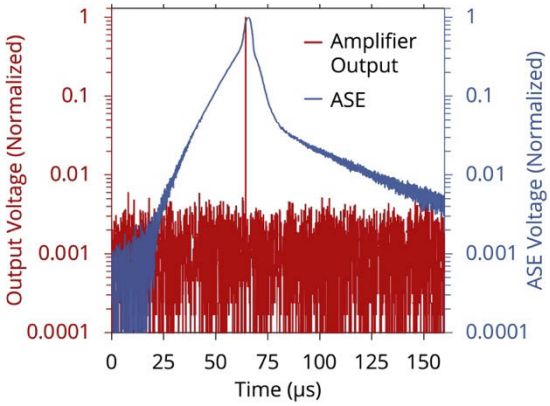

Fig. 2. Pulse contrast measurement showing the amplifier output (red) and ASE (blue). The measurements were taken in different locations and are not on the same scale. The ASE pulse is not visible above the electronic background noise of the red trace, indicating a pulse contrast >100.

After eight passes, the pulse energy is 6.08 mJ, as shown in Fig. 3(b), which agrees with the estimated value. A small-signal single-pass gain of 4.0 and a total gain of ~4,000 are achieved with an average single-pass gain per pass greater than 3. At 7°C, the aforementioned seven-pass

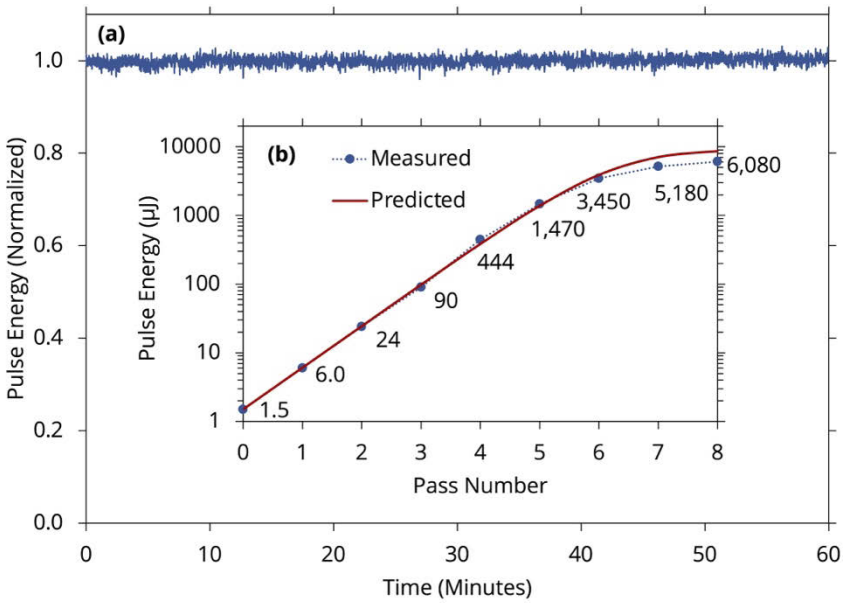

Fig. 3. (a) Long-term power fluctuation measurement. Root-mean-square error was measured to be 0.95% of the average. (b) Measured pulse energy versus pass number and predicted pulse energy based on the Frantz-Nodvik equation.

Optics EXPRESS

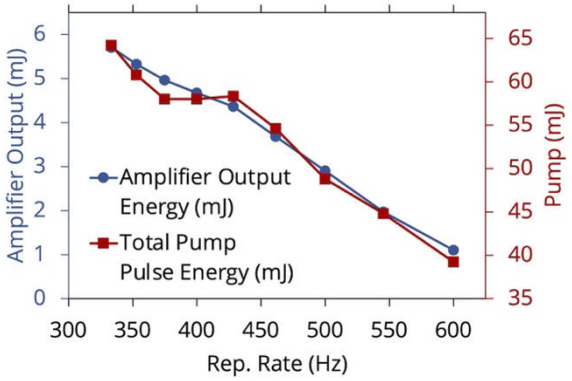

Fig. 4. Eight-pass amplifier output and pump pulse energy at different repetition rates.

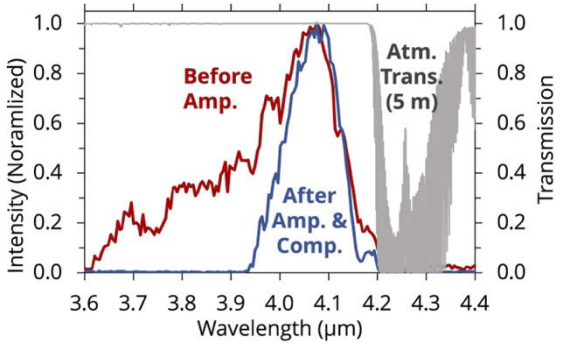

Fig. 5. Spectra before and after amplification with 5 meters of atmospheric CO_2 absorption denoted for reference. After amplification and compression (blue), the spectrum is centered at 4.07 μm. Measured using an APE spectrometer.

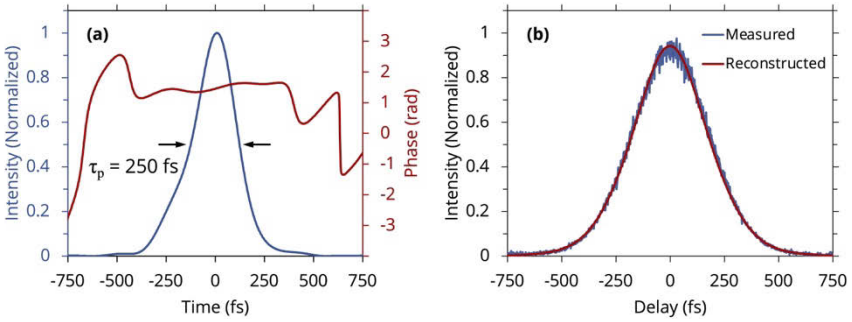

Fig. 6. (a) Pulse shape and phase retrieved from PENGUIN. (b) Comparison of the intensity autocorrelation traces between the one reconstructed based on the pulse shape in (a) and the one measured using an APE autocorrelator.

Optics EXPRESS

CPA achieved a total gain of just 1,125. The single-pass gain at the final pass is 1.17, indicating that the gain medium is not yet fully saturated. The peak fluence of the laser beam in the final pass is 77 mJ/cm^2, which is below the estimated laser-induced damaged threshold at the duration of the stretched pulse [12]. Figure 4 shows that both the pump pulse energy and the multi-pass amplifier (MPA) output decrease with increasing repetition rate. Therefore, more passes would be needed to increase the repetition rate while maintaining the same output energy. Long-term power stability is good with a root mean square error of 0.95% of the average as shown in Fig. 3(a). By sampling at a rate of 45 ms over 5 minutes, the standard deviation of the pulse energy was found to be 2.84% of the average.

2.3. Results

After compression using a Treacy grating pair (Richardson Gratings), 4.59-mJ pulses at 4.07 μm and 333 Hz were measured. The average power is 1.53 W, which is 44 times higher than the Fe:ZnSe-based CPA operating at near room temperature [12]. Compressor throughput was measured to be 79%. The spectra of the pulses before the multi-pass amplifier and after the compressor are shown in Fig. 5. The spectral bandwidth of the pulse supports a Fourier-transform-limited duration of 237-fs. A FWHM pulse duration of 250 fs was measured using a second harmonic autocorrelator. The pulse shape and spectral phase were retrieved by applying the phase-enabled nonlinear gating with unbalanced intensity (PENGUIN) algorithm, as described in [21], to an unbalanced interferometric autocorrelation trace. The intensity autocorrelation trace was then reconstructed and compared to the measured intensity autocorrelation trace to validate the results as shown in Fig. 6(b).

The output beam is Gaussian-like, with a 1/e^2 diameter of 10 mm. Because of the cryogenic cooling in the crystals, beam quality is excellent with an M^2 value near 1 at the 333 Hz repetition rate, as shown in Fig. 7. The source was able to generate odd harmonics up to the ninth order (~452 nm) when focused in air by a lens with a 40-mm focal length (Fig. 8), indicating its potential for use in strong-field experimentation. Also observed in Fig. 8 is a ~2-μm signal suggesting SHG that occurs somewhere in the system. This signal is weak, and its source is yet unknown; although, it is present before focusing in air.

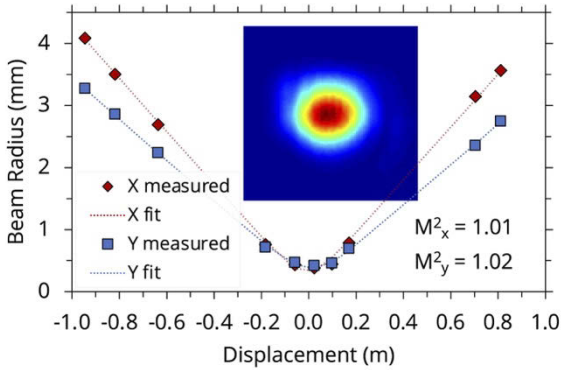

Fig. 7. Beam profile and beam quality after compression. M^2 along the *x* and *y* axes was measured to be 1.01 and 1.02 respectively. Measurements were made using a pyroelectric camera from Ophir-Spiricon.

Optics EXPRESS

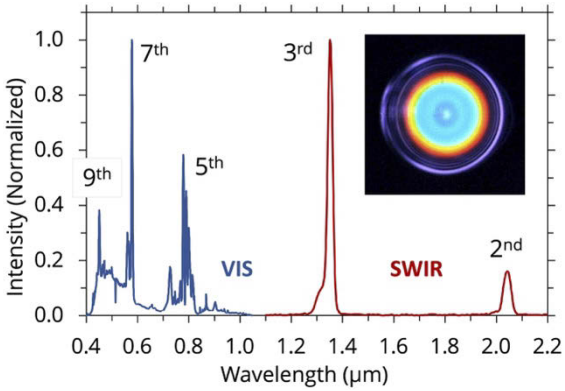

Fig. 8. Spectra of the third (1357 nm), fifth (814 nm), seventh (581 nm), and ninth (452 nm) harmonics generated by tightly focusing the beam in air. A second harmonic signal is also observed at 2.04 μm, the source of which is yet undiscovered. The harmonics spectrum spanned the sensitivity regions of a Si-based (VIS) and an InGaAs-based (SWIR) spectrometer. A color photo of the conical emission from the filament is in the upper right corner of the figure.

3. Conclusions

In conclusion, the advantages of cooling Fe:ZnSe to cryogenic temperature in CPA lasers are validated. High-repetition-rate, free-running Er:YAG lasers originally built for medical applications are used as pump lasers thanks to the increased upper-state lifetime. The 333-Hz repetition rate and 1.53-W average output power of the CPA laser are respectively 33 and 44 times higher than what were previously demonstrated at near-room temperature. Beam quality and power stability are also excellent. Increasing the repetition rate by adding more passes through the amplifier is feasible. The 4.07-μm center wavelength allows all laser components except the gain crystals to be placed in ambient air, instead of in a vacuum chamber, which makes the laser operation much easier. Seeding the CPA by an Yb-laser-pumped OPA is also demonstrated. Such lasers are becoming popular in intense-laser-matter-interaction experiments due to their high efficiency, stability, and reliability. Further compression of output pulses by high-order spectral phase correction and spectral broadening in nonlinear media will be implemented to apply this source to isolated attosecond pulse generation and to the study of MWIR filamentation in the air.

Funding. Defense Threat Reduction Agency (HDTRA11910026); National Science Foundation (2207674); Air Force Office of Scientific Research (FA9550-20-1-0295).

Disclosures. The authors declare no conflicts of interest.

Data availability. Data underlying the results presented in this Letter are not publicly available at this time but may be obtained from the authors upon reasonable request.

References

1. J. Li, J. Lu, A. Chew, S. Han, J. Li, Y. Wu, H. Wang, S. Ghimire, and Z. Chang, "Attosecond science based on high harmonic generation from gases and solids," Nat. Commun. **11**(1), 2748 (2020).
2. X. Ren, J. Li, Y. Yin, K. Zhao, A. Chew, Y. Wang, S. Hu, Y. Cheng, E. Cunningham, Y. Wu, M. Chini, and Z. Chang, "Attosecond light sources in the water window," J. Opt. **20**(2), 023001 (2018).
3. J. Li, X. Ren, Y. Yin, K. Zhao, A. Chew, Y. Cheng, E. Cunningham, Y. Wang, S. Hu, Y. Wu, M. Chini, and Z. Chang, "53-attosecond X-ray pulses reach the carbon K-edge," Nat. Commun. **8**(1), 186 (2017).
4. S. L. Cousin, N. Di Palo, B. Buades, S. M. Teichmann, M. Reduzzi, M. Devetta, A. Kheifets, G. Sansone, and J. Biegert, "Attosecond Streaking in the Water Window: A New Regime of Attosecond Pulse Characterization," Phys. Rev. X **7**(4), 041030 (2017).
5. B. Buades, I. Leon, and N. Di Palo, *et al.*, "Attosecond Soft-X-Ray Spectroscopy of a Transition Metal Dichalcogenide Material," in *Nonlinear Optics (NLO), OSA Technical Digest* (Optical Society of America, 2019), NF1A.5.

Optics EXPRESS

6. N. Saito, H. Sannohe, N. Ishii, T. Kanai, N. Kosugi, Y. Wu, A. Chew, S. Han, Z. Chang, and J. Itatani, "Real-time observation of electronic, vibrational, and rotational dynamics in nitric oxide with attosecond soft x-ray pulses at 400 eV," Optica **6**(12), 1542–1546 (2019).
7. Z. Chang, L. Fang, and V. Fedorov, *et al.*, "Intense infrared lasers for strong-field science," Adv. Opt. Photon. **14**(4), 652 (2022).
8. A. V. Mitrofanov, A. A. Voronin, D. A. Sidorov-Biryukov, S. I. Mitryukovsky, A. B. Fedotov, E. E. Serebryannikov, D. V. Meshchankin, V. Shumakova, S. Ališauskas, A. Pugžlys, V. Y. Panchenko, A. Baltuška, and A. M. Zheltikov, "Subterawatt few-cycle mid-infrared pulses from a single filament," Optica **3**(3), 299–302 (2016).
9. G. Andriukaitis, T. Balčiūnas, S. Ališauskas, A. Pugžlys, A. Baltuška, T. Popmintchev, M.-C. Chen, M. M. Murnane, and H. C. Kapteyn, "90 GW peak power few-cycle mid-infrared pulses from an optical parametric amplifier," Opt. Lett. **36**(15), 2755–2757 (2011).
10. K. Zhao, H. Zhong, P. Yuan, G. Xie, J. Wang, J. Ma, and L. Qian, "Generation of 120 GW mid-infrared pulses from a widely tunable noncollinear optical parametric amplifier," Opt. Lett. **38**(13), 2159–2161 (2013).
11. Y. Fu, B. Xue, K. Midorikawa, and E. J. Takahashi, "TW-scale mid-infrared pulses near 3.3 μm directly generated by dual-chirped optical parametric amplification," Appl. Phys. Lett. **112**(24), 241105 (2018).
12. E. Migal, A. Pushkin, B. Bravy, V. Gordienko, N. Minaev, A. Sirotkin, and F. Potemkin, "3.5-mJ 150-fs Fe:ZnSe hybrid mid-IR femtosecond laser at 4.4 μm for driving extreme nonlinear optics," Opt. Lett. **44**(10), 2550–2553 (2019).
13. J. Evans, T. Harris, E. Turner, M. Kimani, J. M. Mann, R. Stites, G. Cook, and K. Schepler, *Re-absorption and nonradiative energy transfer in vibronic laser gain media, SPIE LASE* (SPIE, 2018), Vol. 10511.
14. N. V. Lugueva and S. M. Luguev, "The Effect of Structural Defects on the Thermal Conductivity of ZnS, ZnSe, and CdTe Polycrystals," High Temp. **42**(1), 54–59 (2004).
15. J. Kernal, V. V. Fedorov, A. Gallian, S. B. Mirov, and V. V. Badikov, "3.9–4.8 μm gain-switched lasing of Fe:ZnSe at room temperature," Opt. Express **13**(26), 10608–10615 (2005).
16. J. Helena, E. D. Maxim, J. Michal, V. David, Š. Jan, N. Michal, K. Václav, A. Z. Yuriy, O. K. Nazar, S. G. Andrey, M. P. Vyacheslav, and V. K. Komar, "Fe:ZnSe laser oscillation under cryogenic and room temperature," Proc. SPIE **8599**, 85990E (2013).
17. E. Migal, A. Pushkin, N. Minaev, B. Bravy, and F. Potemkin, "Control of spectral shift, broadening, and pulse compression during mid-IR self-guiding in high-pressure gases and their mixtures," Opt. Lett. **47**(4), 985–988 (2022).
18. J. Bromage, J. Rothhardt, S. Hädrich, C. Dorrer, C. Jocher, S. Demmler, J. Limpert, A. Tünnermann, and J. D. Zuegel, "Analysis and suppression of parasitic processes in noncollinear optical parametric amplifiers," Opt. Express **19**(18), 16797–16808 (2011).
19. T. Lang, A. Harth, J. Matyschok, T. Binhammer, M. Schultze, and U. Morgner, "Impact of temporal, spatial and cascaded effects on the pulse formation in ultra-broadband parametric amplifiers," Opt. Express **21**(1), 949–959 (2013).
20. P. Ruan, Q. Pan, E. E. Alekseev, S. Y. Kazantsev, L. S. Mashkovtseva, Y. B. Mironov, and S. V. Podlesnikh, "Performance improvement of a Fe2+:ZnSe laser pumped by non-chain pulsed HF laser," Optik **242**, 167005 (2021).
21. A. Gliserin, S. H. Chew, S. Kim, and D. E. Kim, "Complete characterization of ultrafast optical fields by phase-preserving nonlinear autocorrelation," Light: Sci. Appl. **11**(1), 277 (2022).